

A global picture of the S_1/S_0 conical intersection seam of benzene

Quansong Li ^a, David Mendive-Tapia ^b, Martin J. Paterson ^c, Anna Paola Migani ^d,
Michael J. Bearpark ^{b,*}, Michael A. Robb ^b, Lluís Blancafort ^{a,*}

^a*Institut de Química Computacional and Departament de Química, Universitat de Girona, Campus de Montilivi, E-17071 Girona, Spain*

^b*Department of Chemistry, Imperial College London, London SW7 2AZ, U. K.*

^c*School of Engineering and Physical Sciences, Heriot-Watt University, Edinburgh, EH14 4AS, Scotland, U. K.*

^d*Departament de Química Física and Institut de Química Teòrica i Computacional, Universitat de Barcelona and Parc Científic de Barcelona, C/Martí i Franqués 1, E-08028 Barcelona, Spain*

Keywords: *conical intersection seams; benzene; permutational symmetry.*

Abstract. A global picture of the S_1/S_0 intersection seam of benzene is presented. Eleven new conical intersection critical points were located at the CASSCF level, the connectivity was mapped and the energies refined with CASPT2. There are two seam branches related with pairs of degenerate A_{1g}/B_{2u} and E_g states at D_{6h} symmetry, respectively, and the two branches are connected by a seam segment of C_s symmetry. The global energy minimum of the seam is the half-boat shaped intersection that leads to a prefulvenic intermediate (I. J. Palmer, I. N. Ragazos, F. Bernardi, M. Olivucci, M. A. Robb, *J. Am. Chem. Soc.* 115 (1993), 673-682). Several other intersections that can lead to the same intermediate or vibrationally hot benzene lie in a range of 3.7 eV above the global seam minimum. There is a recurrent connectivity pattern where permutationally isomeric seam segments are connected by intersections of a higher symmetry point group.

Dedicated to Professor Horst Köppel on the occasion of his 60th birthday

1. Introduction

Conical intersections play a key role in photochemistry and photophysics [1]. They are not isolated points on the potential energy surface but form part of seams [2] which must be fully understood to grasp all details of the excited-state process. On this premise, we have recently developed seam analysis and characterization methods where the seam is treated as an analogue of a Born-Oppenheimer surface [3]. In these methods, critical points are characterized as minima or saddle points on the seam and can be connected to each other through the analogue of an intrinsic reaction coordinate in the seam [4]. Here we apply this approach to the photophysics and photochemistry of benzene. Benzene is fluorescent at excitation energies close to the band origin of the first excited state, but the fluorescence disappears when it is excited with excess energies of 3000 cm^{-1} or more [5]. The channel responsible for the disappearance of the fluorescence is called channel 3, and it is associated to fulvene, benzvalene and Dewar benzene formation [6]. At higher excess energies, up to the ionization threshold of 9.24 eV (134 nm), photodissociation of vibrationally hot benzene, presumably generated by radiationless decay from the excited state to the ground state, has been made responsible for the formation of several photoproducts [7]. Focusing on channel 3, the photoproducts have been explained to arise from a prefulvenic intermediate that, in its turn, is formed during the decay through a conical intersection [8]. This half-boat shaped intersection, labeled *CI-C_s-I* here, was one of the first conical intersections characterized for an organic molecule, and since then a number of potential energy surface and dynamics studies focusing on channel 3 have followed [9]. Here we will provide a global picture of the seam to complement these studies.

In our analysis we follow two threads. On the one hand, we have located several new conical intersection minima following a systematic approach where we start from highly symmetric structures and descend in symmetry. While some of the structures are very high in energy, some of the new structures are a few eV higher in energy than *CI-C_s-I*, the global minimum of the intersection seam, and could play a role in experiments at higher excitation energies. The other focus of the paper is the connectivity between these structures and its relation with permutational or molecular symmetry. Permutational symmetry is important for a truly global representation of the electronic Hamiltonian of a molecule [10], and its importance for the treatment of non-adiabatic processes has been emphasized in several recent studies [11]. Thus, the low-energy

intersections of benzene described below have several permutational symmetry isomers, as shown exemplarily for $CI-C_s-1$ in Figure 1. These isomers belong to different segments of the seam, and the problem we have addressed is if the segments are connected. In several cases, pairs of permutationally isomeric intersections are connected through higher symmetry intersections. This is analogous to what happens with permutationally isomeric structures on a Born-Oppenheimer potential energy surface. However, in other cases this ‘direct’ connection does not exist because there are no such higher symmetry intersections.

INSERT FIGURE 1 HERE

Computational Details

Computations were carried out at the CASSCF(6,6)/cc-pvdz (complete active space self consistent field with an active space of six electrons in six orbitals) level of theory with a development version of Gaussian [12]. Thirteen conical intersections have been located (see Figure 2). All structures were optimized using symmetry restrictions on the geometry, and critical points on the seam were analyzed calculating the intersection space Hessian [3b]. The relevant orbitals are shown in Figure 3. The connectivity between the conical intersection critical points was established in different ways (see Figure 4). The $CI-C_{2h}-1$ and $CI-C_{2v}$ intersections were connected to $CI-C_s-1$ by running the analogues of intrinsic reaction coordinates (IRC) in the intersection space [4]. The same technique was used to connect $CI-D_{2h}$ to $CI-C_{2h}-1$ and $CI-C_{2v}$. However, in these cases the initial part of the IRC was run freezing the C_1-C_4 distance to 3.9 Å to avoid other states coming below the states of interest (see Figure 1 for the numbering). This constrain was released in the second part of the IRC, which explains the discontinuities observed in Figure 4a,b below. In the case of $CI-C_s-3$ and $CI-C_s-2$, the connection was established by running first a constrained conical intersection with the C_2-C_6 distance fixed to 1.7 Å (it is 1.62 Å at $CI-C_s-3$), and running an intersection space IRC from the constrained optimized point. Moreover, $CI-C_{2h}-2$ and $CI-C_s-5$ were connected by a relaxed conical intersection scan along the C_2-C_6 stretch coordinate (constrained conical intersection optimizations with fixed C_2-C_6 distance); similarly, $CI-C_s-3$ and $CI-C_s-4$ were connected by a relaxed scan with fixed $C_4C_3C_2C_6$ and $C_4C_5C_6C_2$ dihedral angles. To take account of dynamic correlation, the energies were recomputed at the CASPT2

level of theory (no ionization potential electron affinity shift [13] and imaginary level shift of 0.1 a. u. [14]), using Molcas72 [15]. At all intersections, the S_1/S_0 CASPT2 energy gap is of 0.4 eV at most, and the overall changes in the relative energy are small, which suggests that the topology and topography are preserved at that level of theory. The Cartesian coordinates of all conical intersections, including the CASSCF and CASPT2 energies, are presented as Supplementary Data.

Results and Discussion

Conical intersections of high symmetry connecting permutationally isomeric seam segments

To connect permutational symmetry conical intersection isomers, one may start from the conical intersection of interest (*eg* $CI-C_s-I$) and search for an intersection in a point group of higher symmetry (*eg* C_{2v} or C_{2h}). Here we follow a different approach, where we start at the structures of highest symmetry and descend in symmetry to reach the C_s point group. This approach is more systematic and has allowed us to locate 11 new conical intersection critical points. Thus, we start by analyzing the frequencies and normal modes at the minima of D_{6h} symmetry of the ground and first excited state, of A_{1g} and B_{2u} symmetry, respectively. Provided there are no large anharmonicities, one can expect to find a conical intersection seam along the modes where the ground-state frequency is significantly higher than the excited-state one (*ie*, the modes that bring the ground- and excited-state surfaces together). Following these symmetry adapted normal modes, we have located conical intersections of different point group symmetries at the CASSCF level, and analyzed the structures with intersection space frequency calculations. These calculations provide a different set of coordinates from a regular frequency calculation, namely those along which the energy degeneracy is preserved. Moreover, the intersection space modes with imaginary frequencies indicate directions along which lower-energy seam segments can be located. Thus, from the first set of conical intersections, further intersections of lower symmetry can be located following the intersection space modes with imaginary frequencies. The connectivity between seam segments of different point group symmetry can be first assessed correlating the degenerate states, and it is confirmed with the analogue of IRC and relaxed scan calculations in the intersection space (see Computational Details).

INSERT TABLE 1 HERE

In Table 1 we list the normal modes ν_i at the S_1 and S_0 minima of D_{6h} symmetry where the ground-state frequency is larger than the excited-state one, *ie* one can expect to find an S_1/S_0 intersection at geometries sufficiently distorted along those modes. Most of the modes are non-totally symmetric, and in Table 1 we show the point group to which the distorted geometries belong. For clarity, we have added if the distorted geometry is planar or not in ambiguous cases. Following the approach described above, we have been able to locate 8 different intersections (see Table 2, entries a – h, and Figures 2a–h). Four of the crossings ($CI-D_{2h}$, $CI-C_{6v}$, $CI-C_{2h-1}$, $CI-C_{2v}$) involve states that correlate with S_1 and S_0 at D_{6h} symmetry, and the remaining crossings involve different pairs of states. This group of intersections covers most of the cases predicted by our approach, with a few exceptions (see Table 1). In the case of the totally symmetric ν_8 coordinate, S_1 and S_0 approach each other asymptotically along the coordinate but they do not cross because of the anharmonicity of the surfaces. In the case of ν_2 and ν_{10} , our analysis anticipates the existence of an S_1/S_0 seam for planar structures of C_{2h} and C_{2v} point group symmetry. However, this could not be confirmed because other excited states become almost degenerate with the two lowest states and make the location of the degenerate region not possible.

INSERT TABLE 2 HERE

INSERT FIGURE 2 HERE

In Figure 2 we show the different conical intersections and their connectivity. The orbitals involved in the excitations are shown in Figure 3. We first focus on the crossings that belong to the A_{1g}/B_{2u} branch of the seam. At these structures, the states correlate with S_0 and S_1 at the Franck-Condon geometry. The structures are characterized by short C_2-C_6 and C_3-C_5 distances (1.5 – 2.0 Å) (see Figure 1 for the numbering). The structure of highest symmetry of this branch is $CI-D_{2h}$, which has seven imaginary intersection space frequencies. There are two such coordinates of b_{2g} symmetry, and two of b_{3u} symmetry, which lead to $CI-C_{2h-1}$ and $CI-C_{2v}$, respectively. The connectivity has been confirmed by calculating the intersection space IRC that connect $CI-D_{2h}$ with $CI-C_{2h-1}$ and $CI-C_{2v}$ (see Figure 4a,b). The intersection space analysis also suggests that there are lower-energy, planar seam segments of C_{2h} and C_{2v} symmetry (*cf* the imaginary b_{1u} and b_{3g} intersection space frequencies for $CI-D_{2h}$), but

these segments could not be mapped because of the interference of other, close lying excited states. Turning to $CI-C_{2v}$, it has one imaginary intersection space frequency that leads to the $CI-C_s-I$ intersection, as confirmed by an intersection space IRC (Figure 4c). Intersection $CI-C_{2h}-I$ has two imaginary frequencies; the first mode also leads to $CI-C_s-I$, as confirmed again by an intersection space IRC (Figure 4d). The second imaginary frequency leads to structures of C_2 point group symmetry, but additional low lying states have not allowed the study of the intersection space of that point group symmetry. With regard to the topography, the seam segments that connect $CI-C_s-I$ with $CI-C_{2v}$ and $CI-C_{2h}-I$ have a sloped-to-peaked topography, being peaked at $CI-C_s-I$ and sloped at $CI-C_{2v}$ and $CI-C_{2h}-I$. There is also further intersection structure of C_{6v} symmetry that belongs to the A_{1g}/B_{2u} branch (Figure 2d). This intersection has two imaginary intersection space frequencies (Table 2, entry d), including a degenerate mode. One would expect to find lower energy intersections of the D_{3d} , C_{2v} and C_2 point groups along those coordinates. In particular, this intersection should be connected to $CI-C_{2v}$, which belongs to the A_{1g}/B_{2u} branch. However, the study of the connectivity has not been possible here because of the proximity of other excited states.

INSERT FIGURE 3 HERE

The second branch of the seam occurs between a pair of E_g states at the D_{3d} point group symmetry. It occurs for geometries where the hydrogen atoms are highly bent out of the plane. The degenerate state pair correlates with a high-lying excited state at the Franck-Condon geometry. In terms of the π orbitals at D_{6h} symmetry, the configuration is $(a_{2u})^2(e_{2u})^2(b_{2g})^2$. The pair of degenerate e_u orbitals at D_{3d} symmetry is shown in Figure 3e. Intersection $CI-D_{3d}$ (Figure 2e) has two imaginary intersection space frequencies of a_{2u} symmetry that lead to $CI-C_{3v}$. The remaining structures, $CI-C_{3v}$ (E crossing) and $CI-C_{2h}-2$ (A_g/B_g crossing), are local minima on the seam. The three structures have not been connected explicitly because they are very similar in structure and energy, but their similarity indicates that they belong to the same branch. Finally, we have located an intersection of D_2 symmetry (Figure 2h). The intersecting states could not be correlated to those of the remaining cases, which indicates that they correlate with higher-lying states at the other geometries. For this reason, $CI-D_2$ has not been connected to any of the other intersections.

INSERT FIGURE 4 HERE

Low energy conical intersections

In addition to the highly symmetric structures, we have located several conical intersection local minima of C_s symmetry which lie in an energy range of about 2.7 eV from $CI-C_s-1$ (see Figure 2i-m and Table 2i-2m). $CI-C_s-2$ and $CI-C_s-3$ belong to the A_{1g}/B_{2u} branch of the seam, while $CI-C_s-4$ and $CI-C_s-5$ belong to the E_g branch. Three of these structures ($CI-C_s-3$, $CI-C_s-4$ and $CI-C_s-5$) have a fully formed C_2-C_6 bond (see Figure 1 for the numbering). Turning to the connectivity, $CI-C_s-1$ and $CI-C_s-2$ differ only in the pyramidalization of the bridgehead-like carbon atom and are connected by a first-order saddle point in the intersection space [16]; similarly, $CI-C_s-4$ and $CI-C_s-5$ differ in the pyramidalization at C_1 and C_4 . The connection between $CI-C_s-2$ and $CI-C_s-3$ was confirmed with an intersection space IRC (Figure 4e, see Computational Details), while the connection between $CI-C_s-5$ and $CI-C_{2h}-2$ was confirmed by a relaxed scan with frozen C_2-C_6 distances (Figure 4f, see Computational Details). Finally, structures $CI-C_s-3$ and $CI-C_s-4$ could also be connected via a relaxed scan with frozen $C_4C_3C_2C_6$ and $C_4C_5C_6C_2$ dihedral angles (Figure 4g and Computational Details). This scan has a minimum because it goes through geometries close to $CI-C_s-1$. The connection between $CI-C_s-3$ and $CI-C_s-4$ shows that the A_{1g}/B_{2u} and E_g branches of the S_1/S_0 seam are linked by a seam segment of C_s symmetry.

Connectivity between permutationally isomeric segments

We have also analyzed the connectivity between permutationally isomeric segments. There is a frequent pattern where the high-symmetry intersections are saddle points between permutationally isomeric seam segments of lower point group symmetry. This is illustrated in Figure 5 for $CI-D_{2h}$, which connects permutationally symmetric segments of the C_{2v} seam. In the two-dimensional space of the plot, spanned by an in-plane and an out-of-plane bending coordinate (Q_{a1g} and Q_{b2g} , respectively), the seam has a quasi-parabolic topology that reflects the curvature of the seam, in accordance with our second-order model of conical intersection seams [2c,3b]. While this type of connectivity between permutationally isomeric segments is found in several cases, it is not completely general. Thus, the isomeric segments of C_{6v} symmetry are not connected by a D_{6h} structure because there is no seam of that point group symmetry. Instead the isomeric C_{6v} segments could be connected through lower symmetry segments, but this could not be investigated because of the interference of other excited states.

INSERT FIGURE 5 HERE

Conclusions

The S_1/S_0 intersection space of benzene has been mapped by locating 13 minimum energy conical intersections of different point group symmetries. This provides a global picture of the intersection seam. There are two distinct S_1/S_0 seam branches: the A_{1g}/B_{2u} branch, where the intersecting states correlate with S_0 and S_1 at the FC geometry, and the E_g branch at highly twisted geometries. The two branches are connected by an A''/A' seam segment of C_s symmetry mapped out between $CI-C_s-3$ and $CI-C_s-4$. From the point of view of energy, the global intersection space minimum is the ‘classic’ half-boat structure $CI-C_s-1$. In addition to that, there is a group of low-energy intersections in a range of up to 7.6 eV from the FC minimum. Some of these intersections are associated to formation of the pre-fulvenic intermediate described previously [6a,8], with a partially or fully formed 1,3 carbon-carbon bond across the ring, and they could be reached experimentally at 165 nm or shorter excitation wave lengths. In the same energy range, however, there are sloped seam segments associated to $CI-C_{2v}$ and $CI-C_{2h}-1$ that could also be populated, leading to decay without primary photoreactivity. A similar sloped, high-energy seam region near $CI-C_s-1$ was recently described in the context of reactivity control for benzene [9e]. Between 1.0 and 1.5 eV higher in energy (excitation wave lengths approximately 140 nm or shorter), the highly twisted structures of the E_g branch could be reached. Decay at these structures would probably produce highly vibrationally excited benzene, without direct bond breaking or formation of any new bonds. This would be in agreement with the proposed photolysis mechanisms that involve vibrationally hot benzene [7]. A reliable assessment of the experimental relevance of these intersections would require a further, accurate mapping of the surface, including barriers, but this is out of the scope of the present paper. Thus, our main interest is the structure of the seam. Although our analysis of the connectivity between permutationally isomeric seam segments is not comprehensive, since we have only considered isomers with the same atom connectivity, we have found a recurring pattern. Thus, the connectivity is mediated by structures of higher symmetry (see Figure 5). The segments of C_{6v} symmetry are an exception to this trend. They should be connected by a seam of D_{6h} symmetry, but this seam does not exist. Alternatively, the

C_{6v} segments could be connected through segments of lower symmetry, but this could not be studied because of the proximity of other excited states. A general investigation of the topologies formed by connected seam segments of different symmetries will be the subject of further studies.

Acknowledgements. This work has been supported by Grant CTQ2008-06696 from the Spanish Ministerio de Ciencia e Innovación (MICINN). Q. Li acknowledges a Juan de la Cierva fellowship of the MICINN, and A. Migani a Beatriu de Pinós fellowship of the Generalitat de Catalunya (Spain).

References.

- [1] (a) E. Teller, *J. Phys. Chem.* 41 (1937), 109-116; (b) M. Klessinger, J. Michl, *Excited States and Photochemistry of Organic Molecules*, VCH Publishers, Inc., New York, 1995; (c) F. Bernardi, M. Olivucci, M. A. Robb, *Chem. Soc. Rev.* 25 (1996), 321-328; (d) W. Domcke, D. R. Yarkony, H. Köppel (Eds.), *Conical Intersections: Electronic Structure, Dynamics & Spectroscopy*, Advanced Series in Physical Chemistry, vol. 15, World Scientific, Singapore, 2004; (e) L. Blancafort, F. Ogliaro, M. Olivucci, M. A. Robb, M. J. Bearpark, A. Sinicropi, in: A. G. Kutateladze (Ed.) *Computational Methods in Photochemistry, Molecular and Supramolecular Photochemistry*, vol. 13, Taylor & Francis, Boca Raton, FL, 2005, pp. 31-110; (f) D. R. Yarkony, *Rev. Mod. Phys.* 68 (1996), 985-1013.
- [2] (a) G. J. Atchity, S. S. Xantheas, K. Ruedenberg, *J. Chem. Phys.* 95 (1991), 1862-1876; (b) D. R. Yarkony, *J. Chem. Phys.* 123 (2005), 204101; (c) L. Blancafort, B. Lasorne, M. J. Bearpark, G. A. Worth, M. A. Robb, in: H. Köppel, D. R. Yarkony, H. Barentzen (Eds.), *The Jahn-Teller Effect. Fundamentals and Implications for Physics and Chemistry*, Springer Series in Chemical Physics, vol. 97, Springer-Verlag, Berlin Heidelberg, 2009, pp. 169-200.
- [3] (a) M. J. Paterson, M. J. Bearpark, M. A. Robb, L. Blancafort, *J. Chem. Phys.* 121 (2004), 11562-11571; (b) F. Sicilia, L. Blancafort, M. J. Bearpark, M. A. Robb, *J. Phys. Chem. A* 111 (2007), 2182-2192.
- [4] F. Sicilia, L. Blancafort, M. J. Bearpark, M. A. Robb, *J. Chem. Theor. Comput.* 4 (2008), 257-266.
- [5] (a) J. H. Callomon, J. E. Parkin, R. Lopezdel, *Chem. Phys. Lett.* 13 (1972), 125-&; (b) D. B. Moss, C. S. Parmenter, *J. Phys. Chem.* 90 (1986), 1011-1014; (c) R. J. Longfellow, D. B. Moss, C. S. Parmenter, *J. Phys. Chem.* 92 (1988), 5438-5449; (d) M. Clara, T. Hellerer, H. J. Neusser, *Appl. Phys. B* 71 (2000), 431-437.
- [6] (a) L. T. Scott, M. Jones, *Chem. Rev.* 72 (1972), 181-202; (b) D. Bryce-Smith, A. Gilbert, *Tetrahedron* 32 (1976), 1309-1326.
- [7] (a) P. Farmanara, O. Steinkellner, M. T. Wick, M. Wittmann, G. Korn, V. Stert, W. Radloff, *J. Chem. Phys.* 111 (1999), 6264-6270; (b) S. T. Tsai, C. K. Lin, Y. T. Lee, C. K. Ni, *J. Chem. Phys.* 113 (2000), 67-70; (c) T. C. Hsu, J. N. Shu, Y. Chen, J. J. Lin, Y. T. Lee, X. M. Yang, *J. Chem. Phys.* 115 (2001), 9623-9626; (d) V. V. Kislov, T. L. Nguyen, A. M. Mebel, S. H. Lin, S. C. Smith, *J. Chem. Phys.* 120 (2004), 7008-7017.
- [8] (a) I. J. Palmer, I. N. Ragazos, F. Bernardi, M. Olivucci, M. A. Robb, *J. Am. Chem. Soc.* 115 (1993), 673-682; (b) A. L. Sobolewski, C. Woywod, W. Domcke, *J. Chem. Phys.* 98 (1993), 5627-5641; (c) J. Dreyer, M. Klessinger, *Chem. Eur. J.* 2 (1996), 335-341.
- [9] (a) B. R. Smith, M. J. Bearpark, M. A. Robb, F. Bernardi, M. Olivucci, *Chem. Phys. Lett.* 242 (1995), 27-32; (b) A. Toniolo, A. L. Thompson, T. J. Martinez, *Chem. Phys.* 304 (2004), 133-145; (c) G. A. Worth, *J. Photochem. Photobiol., A* 190 (2007), 190-199; (d) G. A. Worth, R. E. Carley, H. H. Fielding, *Chem. Phys.* 338 (2007), 220-227; (e) B. Lasorne, M. J. Bearpark, M. A. Robb, G. A. Worth, *J. Phys. Chem. A* 112 (2008), 13017-13027; (f) B. Lasorne, F.

- Sicilia, M. J. Bearpark, M. A. Robb, G. A. Worth, L. Blancafort, *J. Chem. Phys.* 128 (2008), 124307; (g) D. S. N. Parker, R. S. Minns, T. J. Penfold, G. A. Worth, H. H. Fielding, *Chem. Phys. Lett.* 469 (2009), 43-47; (h) T. J. Penfold, G. A. Worth, *J. Chem. Phys.* 131 (2009), 064303.
- [10] S. P. Keating, C. A. Mead, *J. Chem. Phys.* 82 (1985), 5102-5117.
- [11] (a) S. Al-Jabour, M. Baer, O. Deeb, M. Leibscher, J. Manz, X. Xu, S. Zilberg, *J. Phys. Chem. A* 114 (2010), 2991-3010; (b) B. Lasorne, M. A. Robb, H.-D. Meyer, F. Gatti, *Chem. Phys.* in press; (c) X. Zhu, D. R. Yarkony, *J. Chem. Phys.* 132 (2010), 104101.
- [12] M. J. Frisch, G. W. Trucks, H. B. Schlegel, G. E. Scuseria, M. A. Robb, J. R. Cheeseman, J. A. Montgomery, Jr., T. Vreven, G. Scalmani, B. Mennucci, V. Barone, G. A. Petersson, M. Caricato, H. Nakatsuji, M. Hada, M. Ehara, K. Toyota, R. Fukuda, J. Hasegawa, M. Ishida, T. Nakajima, Y. Honda, O. Kitao, H. Nakai, X. Li, H. P. Hratchian, J. E. Peralta, A. F. Izmaylov, K. N. Kudin, J. J. Heyd, E. Brothers, V. Staroverov, G. Zheng, R. Kobayashi, J. Normand, J. L. Sonnenberg, F. Ogliaro, M. Bearpark, P. V. Parandekar, G. A. Ferguson, N. J. Mayhall, S. S. Iyengar, J. Tomasi, M. Cossi, N. Rega, J. C. Burant, J. M. Millam, M. Klene, J. E. Knox, J. B. Cross, V. Bakken, C. Adamo, J. Jaramillo, R. Gomperts, R. E. Stratmann, O. Yazyev, A. J. Austin, R. Cammi, C. Pomelli, J. W. Ochterski, P. Y. Ayala, K. Morokuma, G. A. Voth, P. Salvador, J. J. Dannenberg, V. G. Zakrzewski, S. Dapprich, A. D. Daniels, M. C. Strain, O. Farkas, D. K. Malick, A. D. Rabuck, K. Raghavachari, J. B. Foresman, J. V. Ortiz, Q. Cui, A. G. Baboul, S. Clifford, J. Cioslowski, B. B. Stefanov, G. Liu, A. Liashenko, P. Piskorz, I. Komaromi, R. L. Martin, D. J. Fox, T. Keith, M. A. Al-Laham, C. Y. Peng, A. Nanayakkara, M. Challacombe, W. Chen, M. W. Wong, J. A. Pople, *Gaussian Development Version, Revision G.03, Development Version, Revision G.03*, Gaussian, Inc., Wallingford CT, 2008.
- [13] G. Ghigo, B. O. Roos, P. A. Malmqvist, *Chem. Phys. Lett.* 396 (2004), 142-149.
- [14] N. Forsberg, P.-Å. Malmqvist, *Chem. Phys. Lett.* 271 (1997), 196-204.
- [15] G. Karlstrom, R. Lindh, P. A. Malmqvist, B. O. Roos, U. Ryde, V. Veryazov, P. O. Widmark, M. Cossi, B. Schimmelpfennig, P. Neogrady, L. Seijo, *Computational Materials Science* 28 (2003), 222-239.
- [16] S. Maeda, K. Ohno, K. Morokuma, *J. Chem. Theor. Comput.* 6 (2010), 1538-1545.

FIGURE LEGENDS

Figure 1. Permutational symmetry isomers for the half-boat shaped lowest-energy S_1/S_0 conical intersection $CI-C_s-I$ of benzene.

Figure 2. Conical intersection critical points of different point group symmetries (relative energy in eV in square brackets). Arrows reflect mapped connections between the points (see text).

Figure 3. Orbitals involved in the excitations for all conical intersection points, labelled by symmetry.

Figure 4. Energy profiles between different pairs of conical intersection structures (see Computational Details).

Figure 5. Two dimensional model plot of the quasi-parabolic seam formed by two permutationally symmetric seam segments of C_{2v} symmetry connected at $CI-D_{2h}$.

Table 1. Normal modes at the S_0 and S_1 minima of benzene where the frequency of S_0 is significantly larger than S_1 .

Mode	Symmetry	ν_{S_0} [cm^{-1}]	ν_{S_1} [cm^{-1}]	Point group of distorted structure
ν_1	e_{2u}	429	295	D_2, C_{2v} (non planar)
ν_2	e_{2g}	650	578	D_{2h}, C_{2h} (planar)
ν_3	a_{2u}	706	527	C_{6v}
ν_4	b_{2g}	719	487	D_{3d}
ν_5	e_{1g}	867	595	C_{2h} (non planar)
ν_6	e_{2u}	986	674	D_2, C_{2v} (non planar)
ν_7	b_{2g}	1021	700	C_{3v}
ν_8	a_{1ug}	1041	968	D_{6h}
ν_{10}	e_{1u}	1106	961	C_{2v} (planar)

Table 2. Symmetry restricted conical intersection energy minima of different point groups and imaginary intersection space frequencies.

Entry	CI structure	E_{rel}^a [eV]	Irreps of intersecting states	Number and symmetry of imaginary intersection space frequencies	Symmetry of distorted geometries
a	<i>CI-D_{2h}</i>	18.9	A_g/B_{2u}	7 ($2b_{2g}$, $2b_{3u}$, b_{1u} , $2b_{3g}$)	C_{2h} (planar and non planar), C_{2v} (planar and non planar)
b	<i>CI-C_{2h}-1</i>	3.5	A_g/A_u	2 (b_u , b_g)	C_s , C_2
c	<i>CI-C_{2v}</i>	1.7	A_1/B_2	1 (b_2)	C_s
d	<i>CI-C_{6v}</i>	15.7	A_1/B_2	2 (b_2 , e)	D_{3d} , C_{2v} (non planar), C_2
e	<i>CI-D_{3d}</i>	3.9	E_g	2 ($2a_{2u}$)	C_{3v}
f	<i>CI-C_{3v}</i>	3.9	E		
g	<i>CI-C_{2h}-2</i>	3.8	A_g/B_g	-	-
h	<i>CI-D₂</i>	5.7	A/B_3	1 (b_3)	C_2
i	<i>CI-C_s-1</i>	0.0	A'/A''	-	-
j	<i>CI-C_s-2</i>	0.3	A'/A''	-	-
k	<i>CI-C_s-3</i>	2.5	A'/A''	-	-
l	<i>CI-C_s-4</i>	2.3	A'/A''	-	-
m	<i>CI-C_s-5</i>	2.5	A'/A''	-	-

^aCASPT2 energies relative to the ground-state energy at the Franck-Condon geometry.

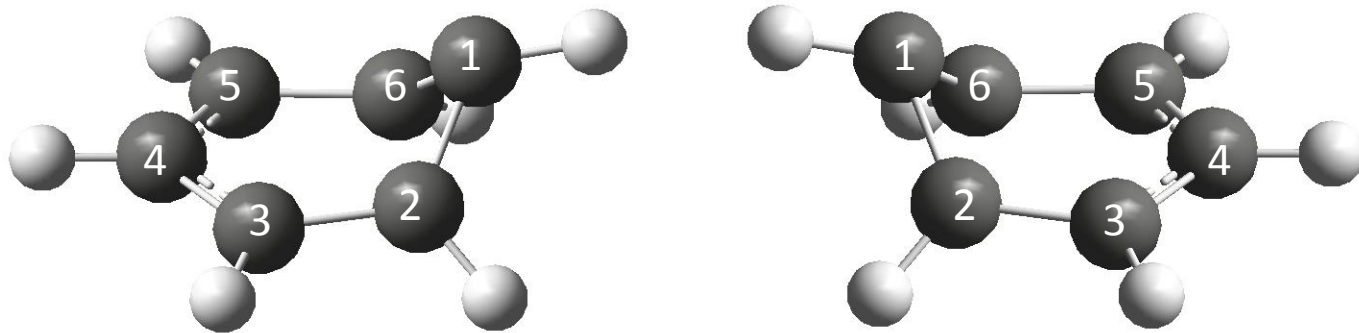


Figure 1.

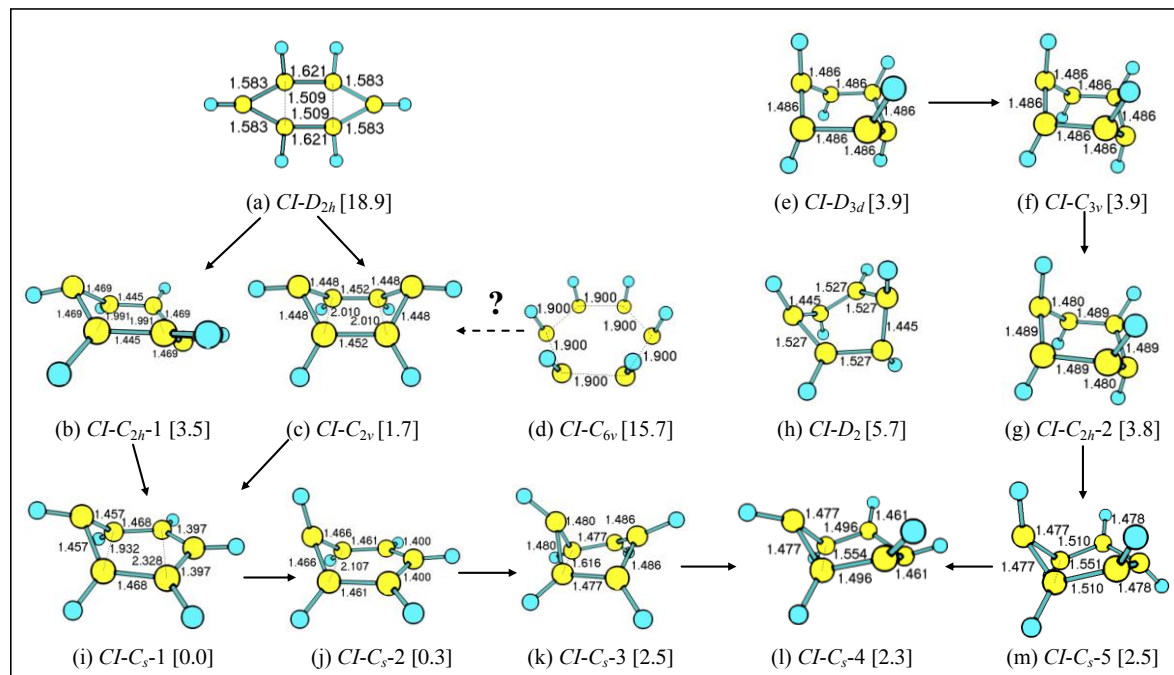
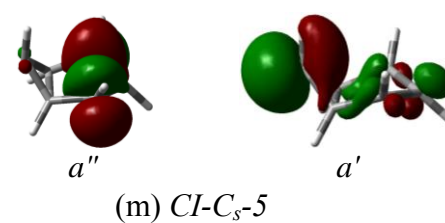
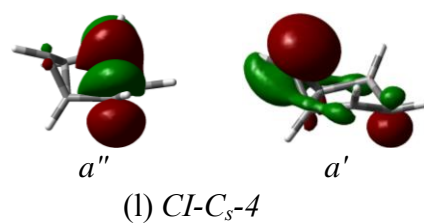
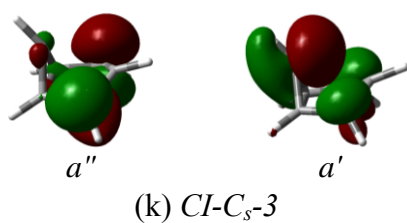
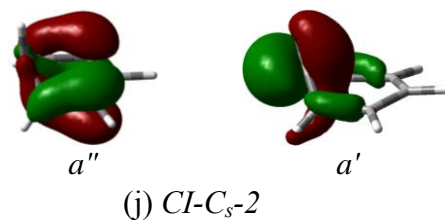
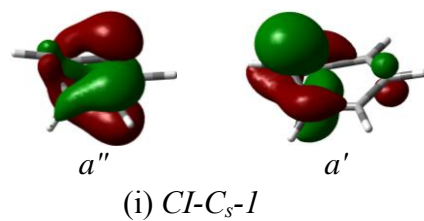
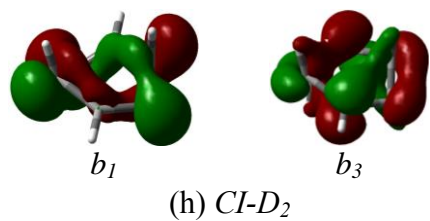
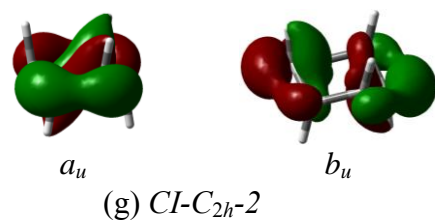
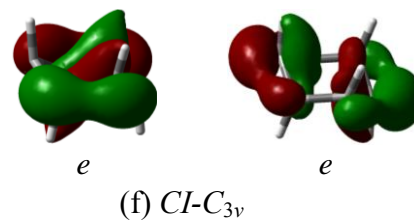
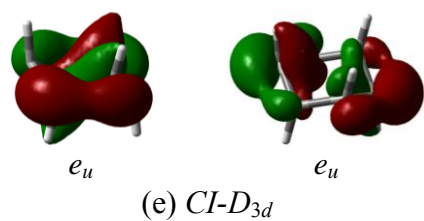
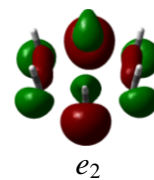
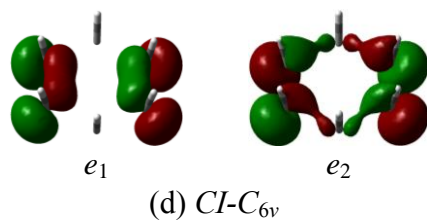
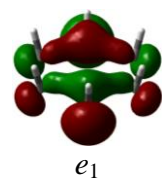
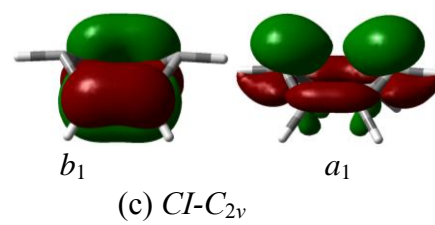
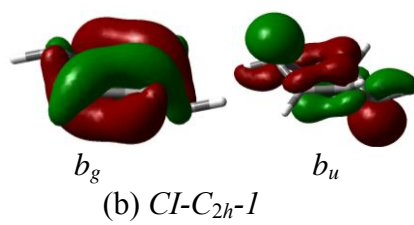
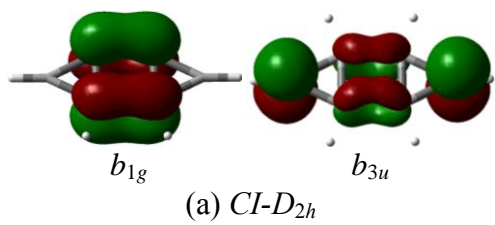
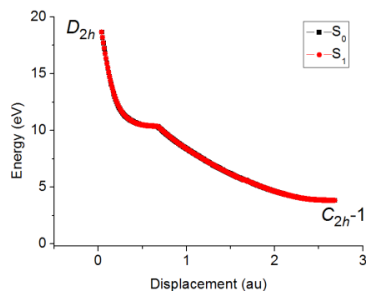


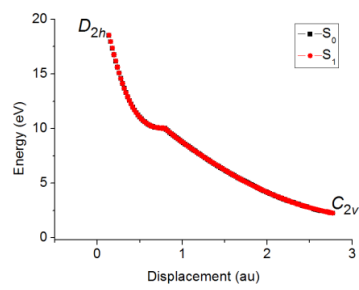
Figure 2.



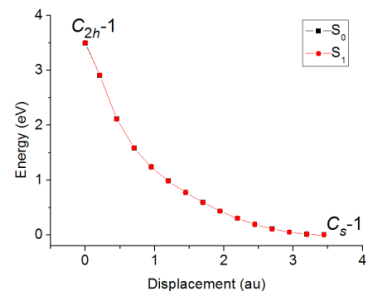
Figure(s)



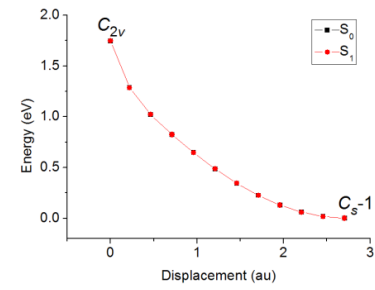
(a)



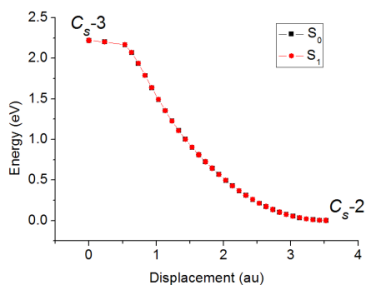
(b)



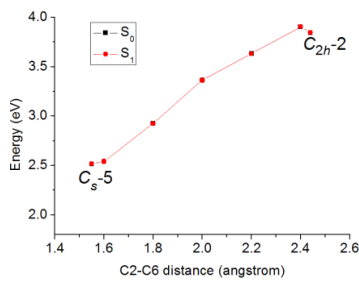
(c)



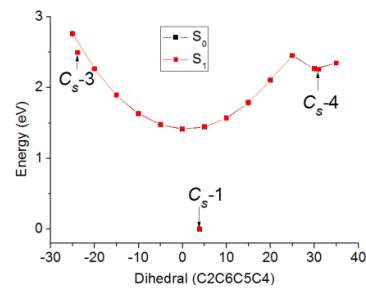
(d)



(e)



(f)



(g)

Figure 4.

Figure(s)

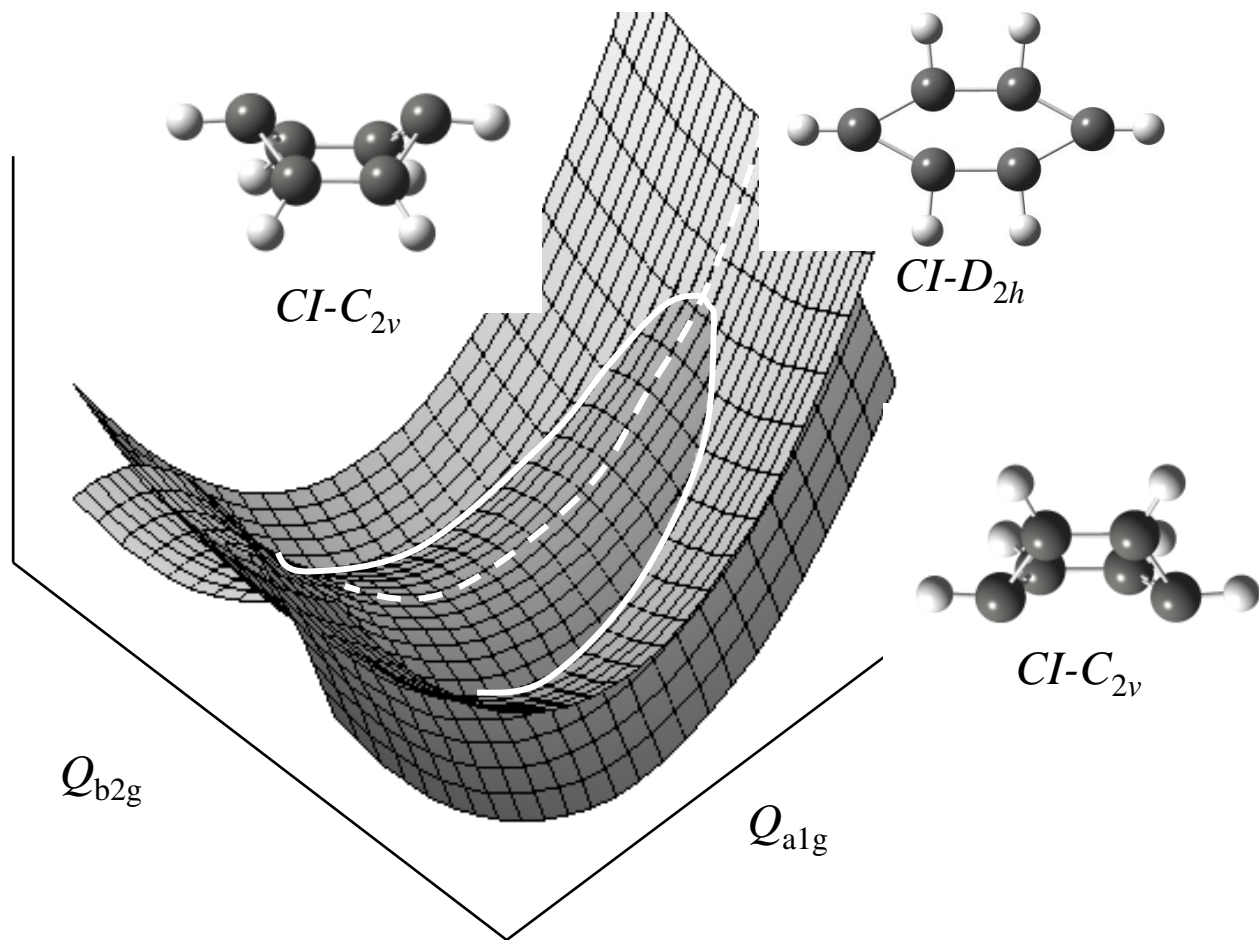


Figure 5